Prediction of volcanic ash concentrations in ash clouds from explosive eruptions based on an atmospheric transport model and the Japanese meteorological satellite Himawari-8: a case study for the Kirishima-Shinmoedake eruption on April 4th 2018

Kensuke Ishii[1*] , Masahiro Hayashi[2], Hiroshi Ishimoto[3] and Toshiki Shimbori[1]

Abstract

Prediction of ash concentrations in volcanic ash clouds for the Kirishima-Shinmoedake eruption on April 4th, 2018 is performed on the basis of an atmospheric transport model and the Japanese meteorological satellite Himawari-8. The retrieval algorithm for Himawari-8 (referred to as the "Optimal Volcanic Ash Algorithm", OVAA) provides two-dimensional properties of volcanic ash clouds, such as cloud heights and total column mass loading, whereas it does not provide ash cloud thickness which is required to make an initial condition for the atmospheric transport model. To estimate ash cloud thickness immediately after an eruption, here, a wind shear index is introduced. The wind shear index includes an empirical constant parameter T_c; a small value of T_c leads to thick ash clouds, whereas a large value of T_c leads to thin ash clouds. In this study, the value of T_c is optimized empirically in the following two ways: (1) a comparison between the total column mass loadings in the prediction and that in the OVAA estimation and (2) a comparison between the estimated ash cloud thickness and the observed ash cloud thickness by lidar measurements. These two comparisons suggest the optimal value of T_c is 0.5−0.6, and then, the uncertainty of the ash clouds thickness estimation to be ∼700 m. In an operation, this estimation of T_c can be used as a fixed value to estimate the ash cloud thickness for a future eruption. In this case, the ash concentration predictions can be obtained immediately after the OVAA estimation. The ash concentrations prediction for T_c=0.6 provides areas of high contamination (>4 mg/m^3) and low contamination (<2 mg/m^3). This classification of ash concentration in ash clouds has been required by the aviation industry, and is helpful information to assess safe areas and routes for airline operations.

Keywords Volcanic ash cloud, Atmospheric transport model, Volcanic ash prediction, Tephra dispersal, Meteorological satellite, Japanese Meteorological Satellite Himawari-8, Optimal Volcanic Ash Algorithm, OVAA
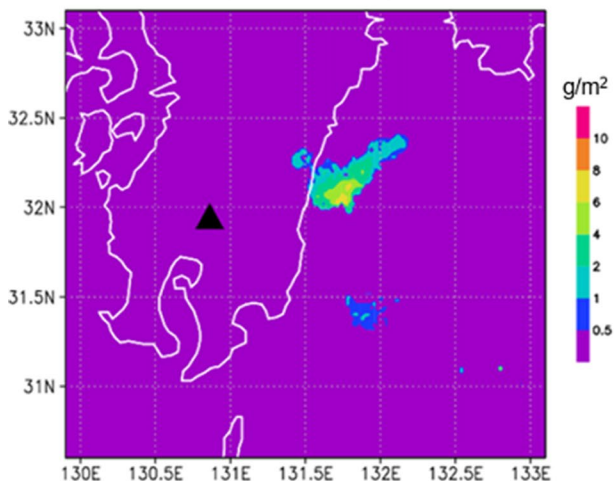
*Correspondence:
Kensuke Ishii
kishii@mri-jma.go.jp
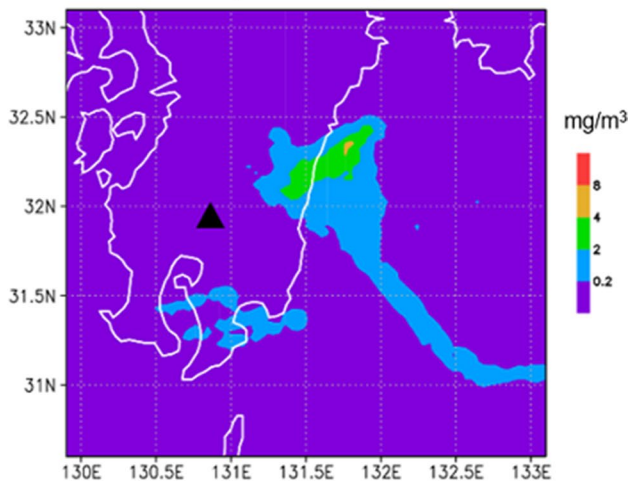Full list of author information is available at the end of the article

Ishii *et al. Earth, Planets and Space* (2023) 75:37

Page 2 of 12

Graphical Abstract

Introduction

Explosive volcanic eruptions inject a large amount of volcanic ash into the atmosphere. Dispersed volcanic ash is one of the most widespread volcanic hazards and has a possibility to cause various impacts, such as on human health, farming, lifelines, and aviation safety (Horwell and Baxter 2006; Wilson and Cole 2007; Barsotti et al. 2010). For example, significant ash emitted from Iceland's Eyjafjallajökull eruption in 2010 was dispersed to an area with high air traffic density over Europe. As a result, the air space over Europe was almost completely closed from April 16 to 21, 2010 causing high losses for airlines (Matthias et al. 2012). Although low ash concentration may not cause crucial damage to the engines of airplanes, no organizations, including the Volcanic Ash Advisory Center, could provide a reliable ash concentration prediction. Therefore, the aviation industry required operational authorities to predict ash concentrations for flying in low concentration ash clouds (Webster et al. 2012).

Numerical atmospheric transport models can help to predict ash concentrations (e.g., Folch 2012). These models calculate the time evolution of ash clouds on the basis of the advection–diffusion–sedimentation (ADS) equation under a realistic atmosphere and an initial distribution of the ash particles (i.e., initial condition). Although some of the models include additional processes, such as aggregation (e.g., Brown et al. 2012) and wet deposition (e.g., Dare et al. 2016), the fundamentals of the models are based on the ADS equation. On the other hand, the

initial conditions are significantly different among the models; some models use the empirical source model (e.g., Suzuki 1983) as the initial condition, and other models use the physical-based eruption source model which includes conservation laws of mass, momentum, and energy (e.g., Costa et al. 2006). The source term often has large uncertainties, and significant efforts have been invested to constrain the source term (e.g., Woods and Bursik 1991; Stohl et al. 2011; Denlinger et al. 2012; Kristiansen et al. 2012; Schmehl et al. 2012). However, even if a perfect source term is obtained, uncertainties in model prediction can still increase with run-time. Therefore, some studies proposed methods to produce an initial condition based on satellite analysis without any eruption source models (e.g., Wilkins et al. 2016). In this case, the initial condition (i.e., source term) for the atmospheric transport model represents ash clouds far from the vent as an effective "virtual source", and is reproduced by the data insertion method and satellite observations of the ash clouds. On the other hand, recent studies of satellite analysis make it possible to estimate the quantitative properties of ash clouds such as the top heights and total column mass loadings (e.g., Pavolonis et al. 2013; Hayashi and Ishimoto 2018). Monitoring by satellites has possible coverage over a wide area, and ash cloud properties estimation are available both day and night for any volcanos in the monitoring area immediately after an eruption. Accordingly, one of the key tasks for ash concentration prediction is to produce an initial distribution of the ash

Ishii *et al. Earth, Planets and Space*   (2023) 75:37

Page 3 of 12

clouds for the atmospheric transport model from satellite analysis.

In this study, we propose a way to predict ash concentration in ash clouds from explosive eruptions, on the basis of the atmospheric transport model and satellite analysis from Himawari-8 (Bessho et al. 2016). In this method, the initial condition for the atmospheric transport model represents ash clouds far from the vent. Although satellite analysis provides the quantitative properties of volcanic ash clouds, such as top heights and total column mass loadings, it does not provide information about the vertical profile such as ash cloud thickness which is an essential parameter to produce the initial condition. In the operation, it is necessary that a prediction is issued as soon as possible. That means that it is vital to estimate the ash cloud thickness to initialize the ash transport model immediately after an eruption. Therefore, ideally, it is hoped that ash cloud thickness can be estimated from the data immediately after an eruption without many time steps. In this study, the ash cloud thickness is estimated by using wind shear. With this method, if the appropriate parameter is obtained in advance, we can estimate the ash cloud thickness immediately after an eruption from one image of Himawari-8 without additional data. The combination of ash cloud properties estimated by a meteorological satellite and empirical estimation of ash cloud thickness makes it possible to produce the initial condition for ash concentration prediction.

Methodology

In this study, ash concentration prediction is composed of the following three processes: an atmospheric transport model, satellite analysis (referred to as the "Optimal Volcanic Ash Algorithm", OVAA), and making the initial condition from the ash cloud properties by OVAA. The step of making the initial condition includes the estimation of the ash clouds thickness.

Atmospheric transport model: JMA–ATM

In this study, we use JMA–ATM (Shimbori and Ishii 2021) as an atmospheric transport model for ash concentrations prediction. JMA–ATM is a Lagrangian model which calculates the dispersion of "model tracers" for real-time ash prediction in JMA's operation (Hasegawa et al. 2015). The physics in JMA–ATM includes mainly advection, diffusion, and sedimentation (ADS). The advection process expresses ash particle transportations by the wind. In this process, we use gridded values in JMA's operational weather forecasting model (JMA–GSM; JMA 2023). The diffusion process expresses the atmospheric turbulence effect in a sub-grid scale (Louis et al. 1982; Gifford 1982, 1984). In this process, the

particle random motions are independent from particle to particle. The sedimentation process is governed by gravitational falling (Suzuki 1983). This process is calculated from the terminal velocity which mainly depends on the particle grainsize. In addition, the initial condition of JMA–ATM have some options for the eruption source term such as an empirical function based on Suzuki (1983). However, in this study, the initial condition is produced on the basis of Himawari-8, and is expressed as the ash clouds far from the vent.

Physical properties of ash clouds from Himawari-8: OVAA

In this study, we adopt an optimal estimation method (e.g., Francis et al. 2012; Pavolonis et al. 2013) which retrieves the ash cloud properties using Himawari-8 IR bands (Bessho et al. 2016). The basic ideas of this method are based on the optimal cloud analysis (OCA; Watts et al. 2011; Otsuka et al. 2021) for meteorological clouds. In this optimal volcanic ash algorithm (OVAA; Hayashi and Ishimoto 2018), the following cost function J is minimized to obtain the parameters x (e.g., optical thickness of ash cloud, effective radius, cloud top height, and skin temperature):

$$J = (x - x_a)^{\mathrm{T}} S_a^{-1} (x - x_a) + \left[f(x) - y_o \right]^{\mathrm{T}} S_y^{-1} \left[f(x) - y_o \right] \tag{1}$$

where x_a is the prior for x, y_o is the observed brightness temperature of Himawair-8 Bands 13, 14, 15 and 16, S_a and S_y are the error covariance matrix for the prior and observation, respectively (see Additional file 1: Tables S1 and S2 in the additional materials for details). $f(x)$ is the forward model to simulate observations under the assumption that scattering objects are volcanic ash particles.

Temperature and water vapor profiles from the JMA–GSM (JMA 2019) is used as inputs of a radiative transfer model (RTTOV-12; Saunders et al. 2018) for the computations of clear-sky components in $f(x)$. OVAA considers the two types of surface emissivities; the sea and land surface. The method proposed by Masuda (2006) is used to compute the sea surface emissivities, whereas the monthly land emissivity atlas (Seemann et al. 2008) was used for the land emissivity. As for the computations of the single scattering properties of volcanic ash, we made the same assumption of volcanic ash particles (shape, size distribution, and refractive index) as Ishimoto et al. (2022); the shape of the volcanic ash was assumed to be a spheroid and the scattering properties were calculated using the T-Matrix method (Mishchenko et al. 2002), whereas a log-normal distribution with a standard deviation of 0.74 was applied for the grainsize distribution of the ash cloud particles. We used the ash refractive index model that adopts a parameterization with the ratio of

non-bridging oxygens to tetrahedrally coordinated cations (NBO/T Prata et al. 2019) to take the ash composition into account. Here, the value of NBO/T in this study is 0.2, which is consistent with the volcanic ash analysis by the hyperspectral sounder observation (Ishimoto et al. 2022) (see Additional file 1: Fig. S1 in the additional materials for details). The total column mass loading is also computed according to the retrieved results (Pavolonis et al. 2013). To detect the volcanic ash, we apply a threshold for the brightness temperature (BT) difference; BT of Band 13–Band 14 < −0.1 K (the reverse absorption method; Prata 1989). We use Band 14 instead of Band 15 which has a longer central wavelength (12.4 μm) band than the traditional 12.0 μm band (e.g., AVHRR Channel 5) usually used for the reverse absorption method (e.g., Prata 1989). This is because the water vapor absorption on Band 15 is larger than the traditional 12.0 μm band (e.g., Murata et al. 2015), hence the ash signal (negative BT difference) tends to be buried especially for thin ash clouds with a BT difference of Band 13–Band 15 which have relatively large positive values (see Additional file 1: Fig. S2 in the additional materials for an example of BT difference).

Initial condition for JMA–ATM

In this study, we produce the initial condition for JMA–ATM by data insertion (Wilkins et al. 2016). In this method, each pixel identified as ash clouds by OVAA is treated as the source term, and source mass is given on the basis of the total column mass loadings by the OVAA. The ash particles as the source term are located uniformly between the bottom and top heights of the ash clouds. In a previous study, the ash cloud thickness is determined from the direct observations of the ash clouds, such as by aircraft lidar (e.g., Wilkins et al. 2014). However, in real-time operation, it is not common to obtain the observed ash cloud thickness. Actually, OVAA does not provide the ash cloud thickness. The uncertainty of ash cloud thickness causes uncertainties in ash cloud prediction, because the advection direction of an ash cloud is governed by the wind which strongly depends on the altitude. Therefore, ash cloud thickness is a key parameter to produce the initial condition.

We propose a method to empirically estimate ash cloud thickness by considering the wind shear in the ash clouds. The fundamental idea of this estimation is based on the assumption that ash clouds are thick at altitudes with weak wind shear, whereas ash clouds are thin at altitudes with strong wind shear. To express this assumption, we introduce a monotonically decreasing function for downward altitude as a wind shear index. The stronger

the wind shear, the more the function decreases. Here, the wind shear index $T(z_1, z_2)$ to evaluate the wind shear strength between the two altitudes of z_1 and z_2 ($> z_1$) is defined as follows:

$$T(z_1, z_2) = \exp\left[-C \int_{z_1}^{z_2} \left|\frac{d\boldsymbol{v}(z)}{dz}\right| dz\right] \tag{2}$$

where $\boldsymbol{v}(z)$ is the horizontal wind vector at the altitude z, $\frac{d\boldsymbol{v}(z)}{dz}$ is the wind shear, and z_2 is the ash cloud top height obtained by OVAA. Here, C ($= 0.1$) [s/m] is the factor introduced to assess the strength of the wind shear in the consideration of the typical atmospheric condition; i.e., $|\frac{d\boldsymbol{v}}{dz}|$ is roughly $0.001 - 0.01$[1/s] ($|d\boldsymbol{v}| \sim 1 - 10$[m/s] for $dz \sim 1$[km]) for typical atmospheric condition. The ash clouds thickness is estimated by solving $T(z_1, z_2) = T_c$ for z_1, where T_c is the constant parameter determined empirically; a large T_c leads to thin ash clouds, whereas a small T_c leads to thick ash clouds. If a certain value of T_c is applicable for many eruption cases, the ash cloud thickness can be estimated immediately after the eruption in operation using the value of T_c.

It should be noted that this simple and empirical method is tentative to estimate the ash cloud thickness for real-time operation immediately after an eruption. The fundamental idea of this method does not consider various conditions other than atmospheric conditions, such as eruption conditions (type, duration, size, etc.), and altitudes of ash clouds. Therefore, a more sophisticated method considering those conditions would improve the estimation. The sophistication of this method will be the focus of the next phase of this study. In the current study, we will show that this method with a certain value of T_c causes the ash cloud thickness estimation to be roughly consistent with the observation in some eruption cases, in spite of the significant simplification.

Application to the 2018 Kirishima-Shinmoedake Eruption

Shinmoedake is an active andesitic stratovolcano, and forms part of the Kirishima volcanic complex in Kyushu, Japan which comprises more than 20 volcanic edifices. In the past 20 years, Shinmoedake experienced a major eruption in 2011, and effusive and explosive eruptions in 2017 and 2018. Various previous studies reported the 2011 eruption (e.g., Nakada et al. 2013; Kozono et al. 2013); the climactic phase of the 2011 eruption was a mixture of sub-plinian and vulcanian eruptive events, successive lava accumulation (lava dome) within the crater, and a repetition of vulcanian events after dome growth (Nakada et al. 2013).

Ishii *et al. Earth, Planets and Space* (2023) 75:37

Page 5 of 12

This volcano is one of the most active volcanoes in Japan, and caused ash clouds which affected aviation safety many times in 2018 (see Tokyo VAAC website). In particular, an eruption on April 4, 2018 (5th in Japanese local time) was one of the remarkable events which caused the highest plume in recent activities (e.g., Matsumoto and Geshi 2021). In addition, the ash clouds from this eruption were detected clearly by Himawari-8 because of few meteorological clouds being around the volcano. In this study, we focus on this eruption which was composed of two explosive eruptions (JMA 2018a, b); the first eruption plume reached an altitude of 6.4 km at 18:31 UTC, and the second eruption plume reached an altitude of 9.4 km at 18:45 UTC, and the eruptions' duration is approximately a few minutes each. The ash clouds from the two eruptions were clearly detected by Himawari-8, and OVAA provided the physical properties of the ash clouds. In the rest of this section, ash concentrations prediction is performed on the basis of the ash clouds properties estimated by OVAA.

Initial conditions and OVAA estimations

Figure 1a, b shows the ash clouds properties estimated by OVAA. The top heights by OVAA are approximately consistent with JMA's reports including ground-based weather radar observation (JMA 2018a, b; Sato et al. 2018). The total column mass loadings are also estimated by OVAA (Fig. 1a). The OVAA estimation indicates that the total column mass loadings for the first eruption is larger than that for the second eruption, because the ash cloud from the second eruption was elongated by a strong wind shear. Most of the ash particles grainsize estimated by OVAA is under an order of 1–10 μm. This is consistent with the fact that fine ash less of than several tens of microns can stay in ash clouds for hours or days (Mastin et al. 2009). The terminal velocity of fine ash particles (~10 μm) is under an order of 0.01 m/s (e.g., Cheng 2009). Therefore, the altitudes of ash particles have slight changes in short-time prediction (<~10 h). As a result, information about the ash particle grainsize is not important for the short-time prediction. Figure 1c, d shows the wind shear index for the two locations; that for the low ash cloud decreases incrementally due to the weak wind shear (Fig. 1c), whereas that for the high ash cloud decreases rapidly due to the strong wind shear (Fig. 1d).

Figure 2a shows tracers in the initial condition for JMA–ATM which is made from OVAA estimation at 20:30 UTC. The initial condition reproduces the main features of the ash cloud properties by OVAA; the horizontal distribution and top height of the ash cloud. Figure 2b–d shows the vertical cross sections of the initial condition for the three values of T_c (=0.3, 0.6, 0.9) as typical value. A small T_c leads to thick ash clouds (Fig. 2b),

whereas a large T_c leads to thin ash clouds (Fig. 2d). On the other hand, the ash clouds heights do not depend on T_c (Fig. 2b–d), because the top heights estimated by OVAA are used. In the next section, we present ash predictions for the various values of T_c (i.e., the various ash cloud thicknesses), and optimize T_c by comparing JMA–ATM's predictions and the OVAA estimation.

Predictions by JMA–ATM

Figure 3d–l shows the total column mass loadings in the predictions by JMA–ATM for the forecast lead time (FT) of 1–3 h. The initial conditions are produced from the ash cloud properties by OVAA and the ash cloud thickness estimation for the various values of T_c (=0.3, 0.6, 0.9) (see Additional file 1: Fig. S3 in the additional materials for other value of T_c). The ash cloud in the prediction for T_c=0.3 spread to a wide area including the west of the ash cloud area from OVAA (Fig. 3c, f). This result is consistent with the general feature that thick ash clouds are advected by the various wind directions at various altitudes. Therefore, this overestimation of the ash clouds area indicates that the value of T_c should be larger than 0.3 for this case. In contrast, the predictions for T_c =0.6 and 0.9 (Fig. 3g–l) seem to be approximately consistent with the ash cloud area by OVAA. However, the total column mass loadings in the prediction for T_c=0.6 are more consistent with those by OVAA regarding the max value. The total column mass loadings in the prediction (FT=3 h) for T_c=0.9 has a max value over 10 g/m^2 (Fig. 3l) for the max value of the OVAA estimation 6–8 g/m^2 at 23:30UTC (Fig. 3c), whereas that for T_c=0.6 is approximately consistent with that by OVAA (Fig. 3c, i). In addition, the prediction for T_c=0.6 reproduces that the ash clouds are elongated to the east and west, while the max value of the total column mass loading is decreasing during the predicted 3 h. On the other hand, the ash clouds in the prediction for T_c=0.9 maintain the area and the max value of the total column mass loadings in the duration of the model prediction. The overestimation of the max value and the underestimation of the area in the prediction for T_c=0.9 comes from the fact that a thick ash cloud is advected by a single wind direction at a single altitude. Therefore, that indicates that the value of T_c should be smaller than 0.9. Based on the above results, the predictions for $T_c \sim 0.6$ is seemed to be appropriate for OVAA estimation (Fig. 3a–c).

Figure 3m–o shows the ash concentration predictions from the initial condition for T_c=0.6. According to the terminology and standard from ICAO (2021), the ash concentrations in predictions can be classified as "high contamination (>4 mg/m^3)" and "low contamination (<2 mg/m^3)". In particular, the concentrations in the

Ishii *et al. Earth, Planets and Space*   (2023) 75:37

Page 6 of 12
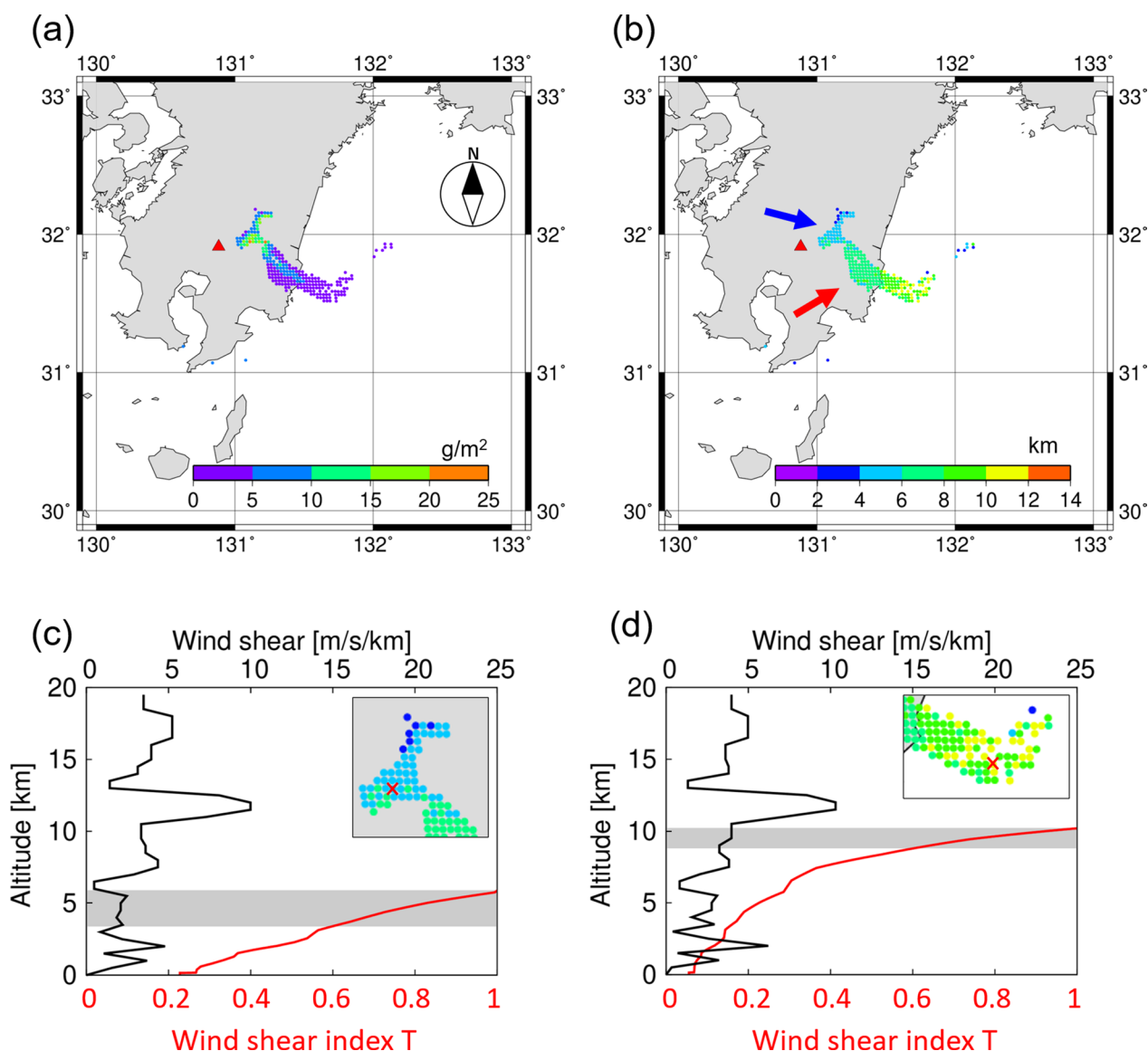
Fig. 1 OVAA outputs at 20:30 on April 4, 2018 (UTC), the wind shear strength $|d\mathbf{v}|/dz$, and the wind shear index. **a** The total column mass loadings estimated by OVAA. **b** The top heights estimated by OVAA. The blue arrow shows the ash cloud from the first eruption (18:31UTC), and the red arrow shows the ash cloud from the second eruption (18:45UTC). **c** Wind shear strength (black line), wind shear index (red line), and estimated ash cloud layer (grey) for Tc=0.6 at N31.970/E131.128 (red cross mark in inset). **d** Same as **c**, but for N31.516/E131.733. The red triangles show the location of the Shinmoedake volcano

prediction for 23:30 UTC (i.e., FT=3 h, Fig. 3o) are under 4 mg/m³ for most of the ash cloud area (i.e., equal to or less than "medium contamination"). This information about the ash concentration is helpful to assess safe areas and routes for airline operation (Clarkson and Simpson 2017).

In this section, T_c (=0.6) was tentatively optimized by comparing the total column mass loadings in the prediction and those in the OVAA estimation. The ash cloud thickness in the initial condition governs the prediction. Therefore, the estimation of the ash clouds thickness is a

key step in ash concentration prediction. In the next section, further discussion of the uncertainty in this estimation will be done using the lidar observation.

Discussion

In this section, we discuss two uncertainties included in the calculation of the ash concentration prediction; the value of T_c and the observation time for OVAA. As explained in the previous sections, T_c governs the ash cloud thickness estimation which is required to make the initial condition for JMA–ATM. Therefore, the

Ishii *et al. Earth, Planets and Space* (2023) 75:37

Page 7 of 12
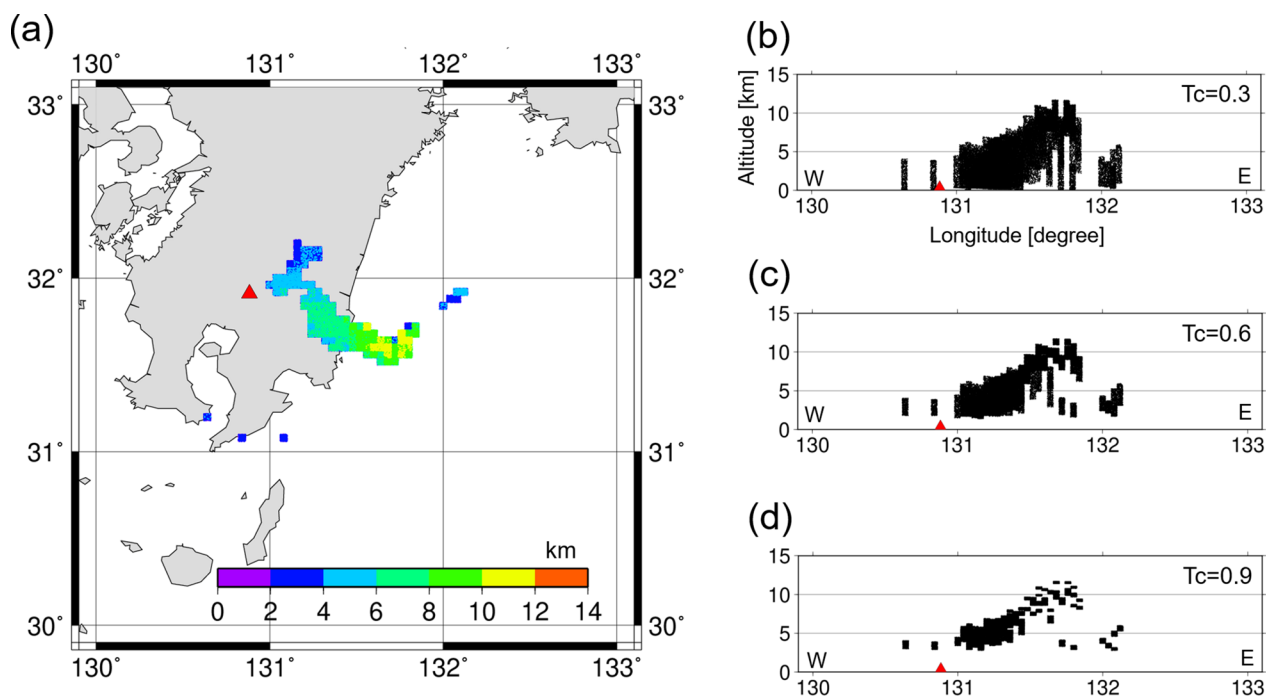
Fig. 2 Initial conditions for JMA–ATM at 20:30 on April 4, 2018 (UTC). **a** The top height of the tracers in the initial condition for JMA–ATM. **b** The vertical cross section of the initial condition for T_c=0.3. **c** Same as **b**, but for T_c=0.6. **d** Same as **b**, but for T_c=0.9

uncertainty in T_c causes the uncertainties in the prediction. Here, T_c is optimized by the observed ash cloud thickness by ground-based and satellite-based lidar. On the other hand, OVAA also has uncertainty relating to the observation time. We can obtain an OVAA estimation every 10 min which is the time interval of the Full Disk image for Himawari-8 (Bessho et al. 2016). Therefore, there are options regarding which observation times for OVAA are used for making the initial condition. Here, we compare the predictions for OVAA estimations at the various observation times.

Empirical parameter T_c

Lidar observation provides the top height and thickness of the ash clouds (e.g., Wang et al. 2008). Here, we assume the top height of the ash clouds by lidar observation as the top height obtained by OVAA, and estimate the ash cloud thicknesses for the various values of T_c (=0.1, 0.2,

0.3,...,0.9). The optimal value of T_c is determined by comparing the estimated thickness and the observed thickness by lidar.

Figure 4 shows the observed ash cloud layers by ground-based and satellite-based lidars (gray) and the wind shear indexes T (red line) for the explosive eruption cases of Mt. Etna in Italy, Mt. Cordon in Chile, Mt. Kasatochi in Alaska, and Mt. Sarychev in Russian (Wang et al. 2008; NASA 2016; Prata et al. 2017). The wind shear indexes in the ash clouds are calculated from the atmospheric conditions of JRA-55C (Kobayashi et al. 2014). As we expected, these results show that the strength of the wind shear roughly corresponds to the ash cloud thickness; for example, the strong wind shear corresponds to the thin ash cloud (e.g., Fig. 4e), and vice versa (e.g., Fig. 4d).

These results (Fig. 4) provide the best values of T_c for each case. The best value of Tc for each case is determined from an intersection between the wind shear

(See figure on next page.)

Fig. 3 **a**–**c** Total column mass loadings estimated by OVAA (21:30, 22:30, 23:30UTC). **d**–**f** The total column mass loadings in the prediction for the T_c=0.3. The forecast lead time (FT) for **d**–**f** are 1, 2 and 3 h, respectively. **g**–**i** Same as **d**–**f**, but for T_c=0.6. **j**–**l** Same as **d**–**f**, but for T_c=0.9. **m**–**o** The ash concentrations predictions in the ash clouds for T_c=0.6. The ash concentrations are calculated from tracers in an unit volume with 0.04 degrees (longitude) × 0.033 degrees (latitude) × 500 m (altitude). The initial time for the prediction (FT=0 h) is set to 20:30UTC (i.e., the initial conditions for JMA–ATM are made from the OVAA estimation at 20:30UTC). The color scale for **a**–**l** is shown next to **c**. The color scale for **m**–**o** is shown next to **o**. The black triangles show the location of the Shinmoedake volcano
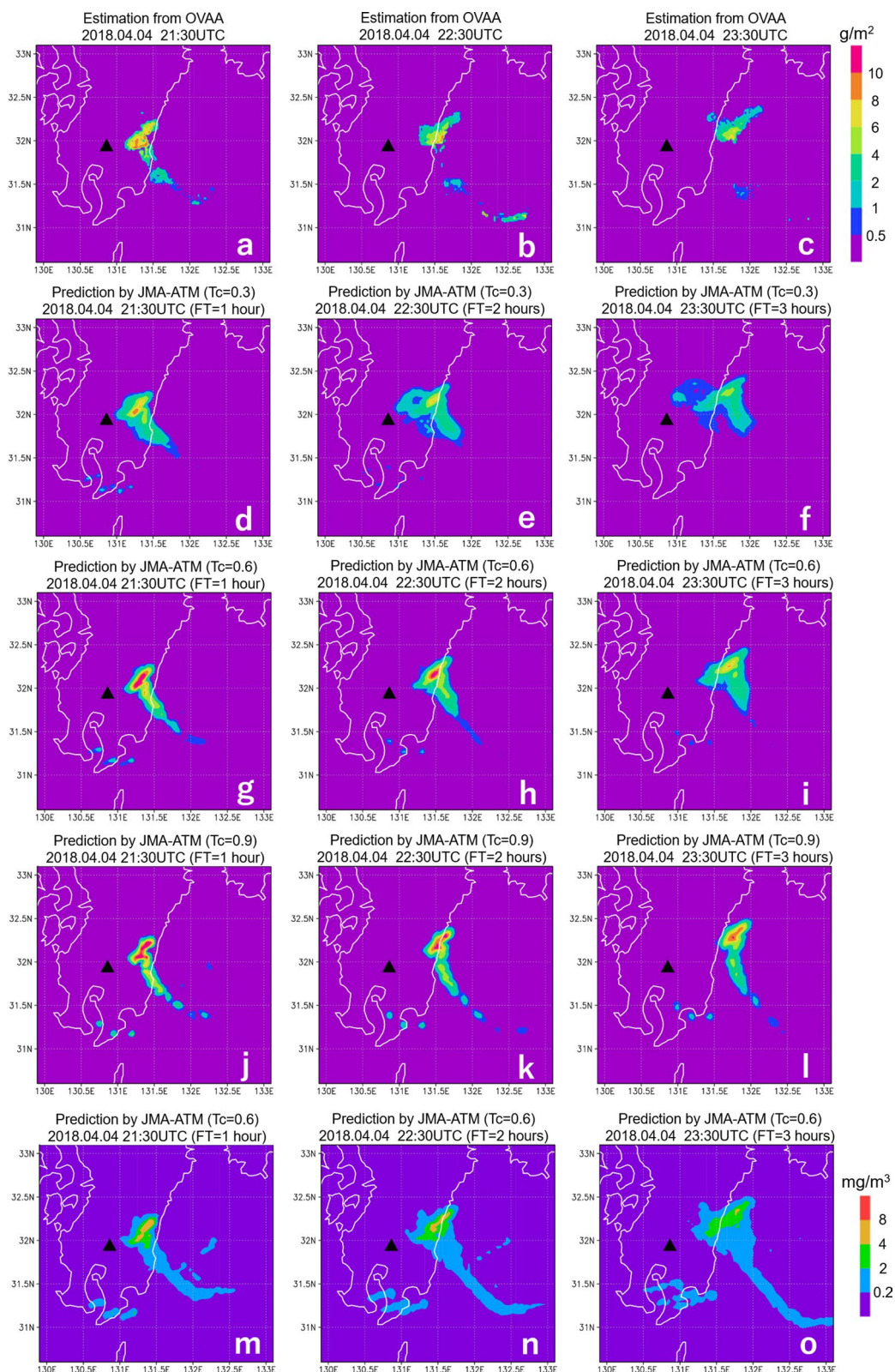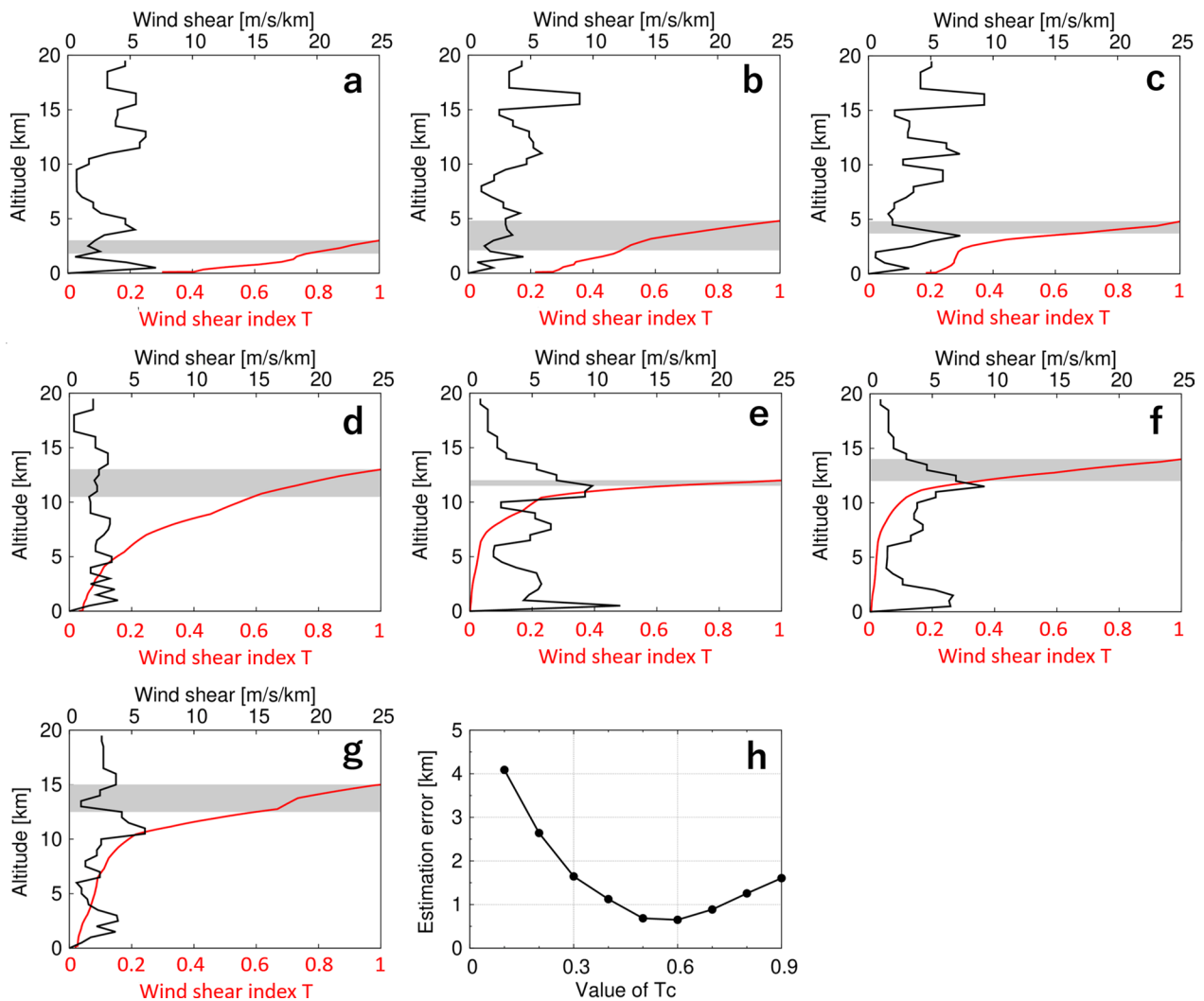
Fig. 3 (See legend on previous page.)

Ishii *et al. Earth, Planets and Space* (2023) 75:37

Page 9 of 12

Fig. 4 Wind shear index *T* (red line), the observed ash clouds layers by lidar (grey), and the wind shear strength |*d****v****/dz*| (black line). **a** The case for 40.838N/14.183E on July 26, 2001. **b** The case for 40.333N/18.1E on July 26, 2001. **c** The case for 40.6N/15.72E on July 25, 2001. **d** The case for 41.76S/168.15E on June 23, 2011. **e** The case for 58.0N/68.56W on August 15, 2008. **f** The case for 56.19N/69.59W on August 15, 2008. **g** The case for 48.11N/178.64E on June 25, 2009. The cases of **a**-**c**, **d**, **e**-**f** and g are for the Mt. Etna eruption in Italy (Wang et al. 2008), the Mt. Cordon eruption in Chile (NASA 2016), the Mt. Kasatochi in Alaska (Prata et al. 2017), and the Mt. Sarychev in Russian (Prata et al. 2017), respectively. **h** The relationship between the standard deviation (i.e., estimation error) and the empirical parameter T_c

index (red line) and the bottom of the ash cloud (grey area): for example, $T_c \sim 0.5$ is the best value for the case of Fig. 4b, because the ash cloud thickness for $T_c=0.5$ is consistent with that from the lidar observation. In addition, these results also show that the wind shear index *T* decreases rapidly downward in strong wind shear (e.g., Fig. 4e), whereas it decreases slowly in the weak wind shear (e.g., Fig. 4d). This tendency of the wind shear index *T* corresponds to the ash cloud thickness estimation; strong wind shear leads to thin ash clouds, whereas the weak wind shear leads to thick ash clouds. Figure 4h shows the standard deviation (i.e., estimation

error) between the estimated thickness and the observed thickness for the 8 cases. This result indicates that that the appropriate value of T_c for these cases is roughly 0.5−0.6 which minimizes the estimation error for the lidar observation, and then, the estimation error is approximately ±0.7 km (±1σ). This value is approximately consistent with the optimal value in the previous section.

Finally, it should be noted that the eruption cases used in this section include various cases, such as a plinian eruption and small eruption. As mentioned in the previous section, this estimation method does not consider

Ishii *et al. Earth, Planets and Space* (2023) 75:37

Page 10 of 12
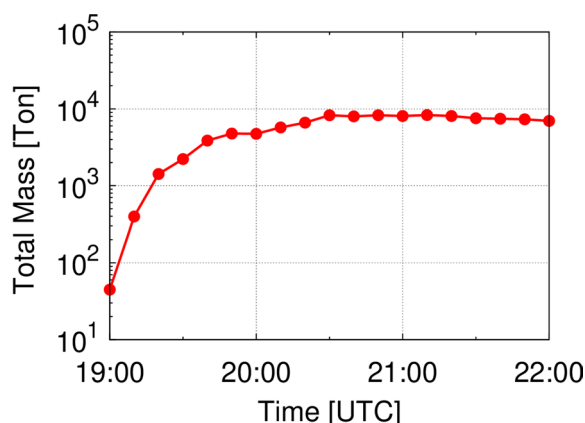
Fig. 5 Time series of the total mass in the ash clouds estimated by OVAA for 19:00–22:00 on April 4, 2018 (UTC)

various conditions, such as eruption type and altitudes of the ash clouds. Therefore, the consideration of the eruption conditions may improve the output of this method.

Observation time of OVAA

For hazard mitigation, ash concentration prediction is required to be calculated and issued as soon as possible after an eruption. In the Himawari-8 operation, Full Disk images are taken every 10 min (Bessho et al. 2016). Therefore, OVAA provides ash cloud properties within 10 min after an eruption. However, unfortunately, OVAA estimation immediately after an eruption cannot be available for prediction.

Figure 5 shows the time series of the total mass in the ash clouds estimated by OVAA for the eruption case in the previous section. The total mass by OVAA increases after the eruption as time, and approaches a certain value asymptotically. Especially, the total mass early immediately after the eruption is significantly underestimated (e.g., 19:00–19:30 UTC). This underestimation is accounted for by the general feature of OVAA that the volcanic ash detection and retrieval scheme of OVAA do not work well for high total column mass loadings. OVAA includes the assumption that the brightness temperature differences between atmospheric window bands are sensitive to detect volcanic ash and to estimate the parameters. However, in the case of an ash plume that is too dense, it is well-known that the ash plume is difficult to detect and the total column mass loading is underestimated by the reverse absorption method (e.g., Prata 2009; Mackie et al. 2016; Prata and Lynch 2019). Therefore, OVAA is not available, or the estimated result is not reliable for ash clouds with high total column mass loadings immediately after an eruption. Actually, in this eruption case, the OVAA estimation immediately after

the eruption causes a serious underestimation in the prediction.

The above discussion suggests that even if the ejected ash is too dense, we can avoid the underestimation in OVAA by monitoring until the total mass in the ash clouds approaches about constant. Actually, in this eruption case, the OVAA estimation is available after 20:30 UTC (i.e., 100 min after the second eruption) when the total mass is approximately constant; the total column mass loadings in the prediction (FT=3 h) based on OVAA estimation at 20:30 UTC is consistent with that from OVAA estimation at 23:30 UTC (Fig. 3c, i).

In general, large eruptions tend to carry coarse pyroclasts to the top of the plume due to the large plume velocity (e.g., Carey and Sparks 1986). Therefore, eruption scale (i.e., mass eruption rate) influences the optical property of the ash clouds for satellite observation, such as grainsize distribution. Although the "decay time" is about 100 min for this case, it may depend on the eruption condition, such as mass eruption rate.

Summary

In this paper, we proposed a way to predict ash concentrations in ash clouds from explosive eruptions on the basis of an atmospheric transport model and satellite analysis (OVAA). OVAA provides the two-dimensional properties of ash clouds, such as the total column mass loadings and the top heights, whereas it does not provide the ash cloud thickness which is a key parameter to make an initial condition for an atmospheric transport model. Therefore, we proposed a way to estimate the ash cloud thickness by the introduction of a wind shear index. This method includes an empirical parameter T_c which governs the estimation result. This empirical parameter T_c was optimized in the following two ways; (1) a comparison between the total column mass loadings in the prediction and those from OVAA at the same time, and (2) a comparison between the estimated thicknesses by the wind shear index and the observed thickness by lidar. As a result, the optimal value of T_c was proposed to be 0.5−0.6. In this case, the uncertainty of the ash clouds thickness was estimated to be about 700 m. The ash concentration prediction was calculated from the initial condition based on the estimation by the OVAA estimation and the ash cloud thickness estimation for T_c=0.6. The prediction classified the concentration in the ash clouds as "high contamination (>4 mg/m^3)" and "low contamination (<2 mg/m^3)". Information about ash concentration is essential to assess safe areas and routes for the aviation industry.

Ishii *et al. Earth, Planets and Space*   (2023) 75:37

Page 11 of 12

Abbreviations
BT   Brightness Temperature
FT   Forecast lead Time
JMA   Japan Meteorological Agency
JMA–ATM Japan Meteorological Agency Atmospheric Transport Model
OVAA   Optimal Volcanic Ash Algorithm

Supplementary Information

The online version contains supplementary material available at https://doi.org/10.1186/s40623-023-01790-y.

<div style="border:1px solid">

Additional file 1: Table S1. Initial values of the parameter x, a-priori value of x_a, and a-priori error covariancematrix (assumed as a diagonal matrix) used in this study. **Table S2.** Observation error covariance matrix S_y (assumed as a diagonal matrix). **Figure S1.** Averages and standard deviations of the cost (the observation term) for eachNBO/T at 20:30 UTC on April 4, 2018. **Figure S2.** Himawari-8 observations at 20:30 on April 4, 2018. **Figure S3.** Same as Figure 3d-f in the main text, but for Tc=0.1.

</div>

Author contributions
The JMA–ATM was developed by TS and KI. The OVAA was developed by MS and HI. The estimation of ash clouds thickness and the prediction of the ash clouds were performed by KI. All authors read and approved the final manuscript.

Availability of data and materials
The data sets of Himawari-8 are available here: https://www.data.jma.go.jp/mscweb/en/product/library_data.html.

Declaration

Competing interests
The authors declare that they have no competing interests.

Author details
[1]Department of Volcanology Research, Meteorological Research Institute, Japan Meteorological Agency, Ibaraki 305-0052, Japan. [2]Department of Typhoon and Severe Weather Research, Meteorological Research Institute, Japan Meteorological Agency, Ibaraki 305-0052, Japan. [3]Department of Observation and Data Assimilation Research, Meteorological Research Institute, Japan Meteorological Agency, Ibaraki 305-0052, Japan.

References
Barsotti S, Andronico D, Neri A, Del Carlo P, Baxter PJ, Aspinall WP, Hincks T (2010) Quantitative assessment of volcanic ash hazards for health and infrastructure at Mt. Etna (Italy) by numerical simulation. J Volcanol Geotherm Res 192:85–96

Bessho K, Date K, Hayashi M, Ikeda A, Imai T, Inoue H, Kumagai Y, Miyakawa T, Murata H, Ohno T, Okuyama A, Oyama R, Sasaki Y, Shimazu Y, Shimoji K, Sumida Y, Suzuki M, Taniguchi H, Tsuchiyama H, Uesawa D, Yokota H, Yoshida R (2016) An introduction to Himawari-8/9 - Japan's new-generation geostationary meteorological satellites. J Meteorol Soc Japan Ser II 94:151–183

Brown RJ, Bonadonna C, Durant AJ (2012) A review of volcanic ash aggregation. Phys Chem Earth Parts A/B/C 45–46:65–78

Carey S, Sparks RSJ (1986) Quantitative models of the fallout and dispersal of tephra from volcanic eruption columns. Bull Volcanol 48:109–125

Cheng NS (2009) Comparison of formulas for drag coefficient and settling velocity of spherical particles. Powder Technol 189:395–398

Clarkson R, Simpson H (2017) Maximising Airspace Use during Volcanic Eruptions: Matching Engine Durability against Ash Cloud Occurrence. Technical Report of NATO-STO MP-AVT-272-17. https://www.sto.nato.int/Pages/default.aspx

Costa A, Macedonio G, Folch A (2006) A three-dimensional Eulerian model for transport and deposition of volcanic ashes. Earth Planet Sci Lett 241:634–647

Dare RA, Potts RJ, Wain AG, (2016) Modelling wet deposition in simulations of volcanic ash dispersion from hypothetical eruptions of Merapi, Indonesia. Atmos Environ 143:190–201

Denlinger RP, Pavolonis MJ, Sieglaff J (2012) A robust method to forecast volcanic ash clouds. J Geophys Res Atmos. https://doi.org/10.1029/2012JD017732

Folch A (2012) A review of tephra transport and dispersal models: Evolution, current status, and future perspectives. J VolcanolGeotherm Res 235–236:96–115

Francis PN, Cooke MC, Saunders RW (2012) Retrieval of physical properties of volcanic ash using Meteosat: A case study from the 2010 Eyjafjallajokull eruption. J Geophys Res Atmos. https://doi.org/10.1029/2011JD016788

Gifford FA (1982) Horizontal diffusion in the atmosphere: A Lagrangian-dynamical theory. Atmos Environ 16:505–512

Gifford FA (1984) The random force theory: Application to meso- and large-scale atmospheric diffusion. Boundary Layer Meteorol 30:159–175

Hasegawa Y, Sugai A, Hayashi Yo, Hayashi Yu, Saito S, Shimbori T (2015) Improvements of volcanic ash fall forecasts issued by the Japan Meteorological Agency. J Appl Volcanol 4:2

Hayashi M, Ishimoto H (2018) Joint Volcanic Ash Retrieval using Himawari-8 and Satellite Infrared Sounder Data. AGU Fall Meeting 2018. https://agu.confex.com/agu/fm18/meetingapp.cgi/Paper/422797

Horwell CJ, Baxter PJ (2006) The respiratory health hazards of volcanic ash: a review for volcanic risk mitigation. Bull Volcanol 69:1–24

International Civil Aviation Organization (ICAO) (2021) Volcanic ash contingency plan. EUR and NAT Documents. https://www.icao.int/EURNAT/EUR

Ishimoto H, Hayashi M, Mano M (2022) Ash particle refractive index model for simulating the brightness temperature spectrum of volcanic ash clouds from satellite infrared sounder measurements. Atmos Meas Tech. https://doi.org/10.5194/amt-15-435-2022

Japan Meteorological Agency (2018a) Monthly volcanic activity report (April 2018) (in English). https://www.data.jma.go.jp/svd/vois/data/tokyo/eng/volcano_activity/monthly.htm

Japan Meteorological Agency (2018b) Monthly volcanic activity report (April 2018) (In Japanese). https://www.data.jma.go.jp/svd/vois/data/tokyo/STOCK/monthly_v-act_doc/fukuoka/18m04/505_18m04.pdf

Japan Meteorological Agency (2023) Outline of the operational numerical weather prediction at the Japan Meteorological Agency. https://www.jma.go.jp/jma/jma-eng/jma-center/nwp/outline2023-nwp/index.htm

Kobayashi C, Endo H, Ota Y, Kobayashi S, Onoda H, Harada Y, Onogi K, Kamahori H (2014) Preliminary Results of the JRA-55C, an atmospheric reanalysis assimilating conventional observations only. SOLA 10:78–82

Kozono T, Ueda H, Ozawa T, Koyaguchi T, Fujita E, Tomiya A, Suzuki YJ (2013) Magma discharge variations during the 2011 eruptions of Shinmoe-dake volcano Japan, revealed by geodetic and satellite observations. Bull Volcanol 75:695

Kristiansen NI, Stohl A, Prata AJ, Bukowiecki N, Dacre H, Eckhardt S, Henne S, Hort MC, Johnson BT, Marenco F, Neininger B, Reitebuch O, Seibert P, Thomson DJ, Webster HN, Weinzierl B (2012) Performance assessment of a volcanic ash transport model mini-ensemble used for inverse modeling of the 2010 Eyjafjallajökull eruption. J Geophys Res Atmos. https://doi.org/10.1029/2011JD016844

Louis JF, Tiedtke M, Geleyn JF (1982) A short history of the PBL parameterization at ECMWF. Workshop on planetary boundary layer parameterization. ECMWF, pp 59-79

Mackie S, Cashman K, Ricketts H, Rust A, Watson M (2016) Volcanic ash: hazard observation. Elsevier, Cambridge, p 288

Mastin LG, Guffanti M, Servranckx R, Webley P, Barsotti S, Dean K, Durant A, Ewert JW, Neri A, Rose WI, Schneider D, Siebert L, Stunder B, Swanson G, Tupper A, Volentik A, Waythomas CF (2009) A multidisciplinary effort

to assign realistic source parameters to models of volcanic ash-cloud transport and dispersion during eruptions. J Volcanol Geotherm Res 186:10–21

Masuda K (2006) Infrared sea surface emissivity including multiple reflection effect for isotropic Gaussian slope distribution model. Remote Sens Environ 103:4

Matsumoto K, Geshi N (2021) Shallow crystallization of eruptive magma inferred from volcanic ash microtextures: a case study of the 2018 eruption of Shinmoedake volcano, Japan. Bull Volcanol 83:31

Matthias V, Aulinger A, Bieser J, Cuesta J, Geyer B, Langmann B, Serikov I, Mattis I, Minikin A, Mona L, Quante M, Schumann U, Weinzierl B (2012) The ash dispersion over Europe during the Eyjafjallajökull eruption - aomparison of CMAQ simulations to remote sensing and air-borne in-situ observations. Atmos Environ 48:184–194

Mishchenko MI, Travis LD, Lacis AA (2002) Scattering, absorption, and emission of light by small particles. Cambridge University Press, Cambridge

Murata H,Takahashi M, Kosaka Y (2015) VIS and IR bands of Himawari-8/AHI compatible with those of MTSAT-2/Imager Meteorological Satellite Center Technical Note 60; pp 1-18

Nakada S, Nagai M, Kaneko T, Suzuki Y, Maeno F (2013) The outline of the 2011 eruption at Shinmoe-dake (Kirishima), Japan. Earth Planets Space 65:475–488

National Aeronautics and Space Administration (NASA) (2016) The NASA Applied Sciences Program: Volcanic Ash Observations and Applications. Annual AMS Meetings (New Orleans, LA). https://ntrs.nasa.gov/citations/20160007811

Otsuka M, Seko H, Hayashi M, Koizumi K (2021) Data Validation and Mesoscale Assimilation of Himawari-8 Optimal Cloud Analysis Products. J Atmos Ocean Technol 38:223–242

Pavolonis MJ, Heidinger AK, Sieglaff J (2013) Automated retrievals of volcanic ash and dust cloud properties from upwelling infrared measurements. J Geophys Res Atmos 118:1436–1458

Prata AJ (1989) Observations of volcanic ash clouds in the 10–12 μm window using AVHRR/2 data. Int J Remote Sens 10:751–761

Prata AJ (2009) Satellite detection of hazardous volcanic clouds and the risk to global air traffic. Nat Hazards 51:303–324

Prata F, Lynch M (2019) Passive earth observations of volcanic clouds in the atmosphere. Atmosphere 10:199

Prata AT, Young SA, Siems ST, Manton MJ (2017) Lidar ratios of stratospheric volcanic ash and sulfate aerosols retrieved from CALIOP measurements. Atmos Chem Phys 17:8599–8618

Prata GS, Ventress LJ, Carboni E, Mather TA, Grainger RG, Pyle DM (2019) A New Parameterization of Volcanic Ash Complex Refractive Index based on NBO/T and SiO2 Content. J Geophys Res Atmos 124:1779–1797

Sato E, Fukui K, Shimbori T, Ishii K, Tokumoto T (2018) Eruption Cloud Echoes from Shinmoe-dake Volcano from March to May, 2018, Observed by JMA Weather Radars. Coordinating Committee for Prediction of Volcanic Eruptions, Japan Meteorological Agency, Tokyo (In Japanese), 130, pp 292-298. https://www.data.jma.go.jp/svd/vois/data/tokyo/STOCK/kaisetsu/CCPVE/Report/130/kaiho_130_38.pdf

Saunders R, Hocking J, Turner E, Rayer P, Rundle D, Brunel P, Vidot J, Roquet P, Matricardi M, Geer A, Bormann N, Lupu C (2018) An update on the RTTOV fast radiative transfer model (currently at version 12). Geosci Model Dev 11:2717–2737

Schmehl KJ, Haupt SE, Pavolonis MJ (2012) A Genetic Algorithm Variational Approach to Data Assimilation and Application to Volcanic Emissions. Pure Appl Geophys 169:519–537

Seemann SW, Borbas EE, Knuteson RO, Stephenson GR, Huang HL (2008) Development of a global infrared land surface emissivity database for application to clear sky sounding retrievals from multi-spectral satellite radiance measurements. J Appl Meteorol Climatol 47:108–123

Shimbori T, Ishii K (2021) Design of the Japan Meteorological Agency Atmospheric Transport Model. Technical Reports of the Meteorological Research Institute 84

Stohl A, Prata AJ, Eckhardt S, Clarisse L, Durant A, Henne S, Kristiansen NI, Minikin A, Schumann U, Seibert P, Stebel K, Thomas HE, Thorsteinsson T, Tørseth K, Weinzierl B (2011) Determination of time- and height-resolved volcanic ash emissions and their use for quantitative ash dispersion modeling: the 2010 Eyjafjallajökull eruption. Atmos Chem Phys 11:4333–4351

Suzuki T (1983) A theoretical model for dispersion of tephra. Physics and Tectonics, Arc Volcanism, pp 95–113

Wang X, Boselli A, D'Avino L, Pisani G, Spinelli N, Amodeo A, Chaikovsky A, Wiegner M, Nickovic S, Papayannis A, Perrone MR, Rizi V, Sauvage L, Stohl A (2008) Volcanic dust characterization by EARLINET during Etna's eruptions in 2001–2002. Atmos Environ 42:893–905

Watts PD, Bennartz R, Fell F (2011) Retrieval of two-layer cloud properties from multispectral observations using optimal estimation. J Geophysl Res Atmos. https://doi.org/10.1029/2011JD015883

Webster HN, Thomson DJ, Johnson BT, Heard IPC, Turnbull K, Marenco F, Kristiansen NI, Dorsey J, Minikin A, Weinzierl B, Schumann U, Sparks RSJ, Loughlin SC, Hort MC, Leadbetter SJ, Devenish BJ, Manning AJ, Witham CS, Haywood JM, Golding BW (2012) Operational prediction of ash concentrations in the distal volcanic cloud from the 2010 Eyjafjallajökull eruption. J Geophys Res Atmos 2012:117

Wilkins KL, Mackie S, Watson IM, Webster HN, Thomson DJ, Dacre HF (2014) Data insertion in volcanic ash cloud forecasting. Ann Geophys. https://doi.org/10.4401/ag-6624

Wilkins KL, Watson IM, Kristiansen NI, Webster HN, Thomson DJ, Dacre HF, Prata AJ (2016) Using data insertion with the NAME model to simulate the 8 May 2010 Eyjafjallajökull volcanic ash cloud. J Geophys Res Atmos 121:306–323

Wilson TM, Cole JW (2007) Potential impact of ash eruptions on dairy farms from a study of the effects on a farm in eastern Bay of Plenty, New Zealand;implications for hazard mitigation. Nat Hazards 43:103–128

Woods AW, Bursik MI (1991) Particle fallout, thermal disequilibrium and volcanic plumes. Bull Volcanol 53:559–570

Publisher's Note